Stress transfer among en echelon and opposing thrusts and tear faults: Triggering caused by the 2003 M_w = 6.9 Zemmouri, Algeria, earthquake

Jian Lin,[1] Ross S. Stein,[2] Mustapha Meghraoui,[3] Shinji Toda,[4] Abdelhakim Ayadi,[5] Catherine Dorbath,[3] and Samir Belabbes[3,6]

[1] The essential features of stress interaction among earthquakes on en echelon thrusts and tear faults were investigated, first through idealized examples and then by study of thrust faulting in Algeria. We calculated coseismic stress changes caused by the 2003 M_w = 6.9 Zemmouri earthquake, finding that a large majority of the Zemmouri afterslip sites were brought several bars closer to Coulomb failure by the coseismic stresses, while the majority of aftershock nodal planes were brought closer to failure by an average of ~2 bars. Further, we calculated that the shallow portions of the adjacent Thenia tear fault, which sustained ~0.25 m slip, were brought >2 bars closer to failure. We calculated that the Coulomb stress increased by 1.5 bars on the deeper portions of the adjacent Boumerdes thrust, which lies just 10–20 km from the city of Algiers; both the Boumerdes and Thenia faults were illuminated by aftershocks. Over the next 6 years, the entire south dipping thrust system extending 80 km to the southwest experienced an increased rate of seismicity. The stress also increased by 0.4 bar on the east Sahel thrust fault west of the Zemmouri rupture. Algiers suffered large damaging earthquakes in A.D. 1365 and 1716 and is today home to 3 million people. If these shocks occurred on the east Sahel fault and if it has a ~2 mm/yr tectonic loading rate, then enough loading has accumulated to produce a M_w = 6.6–6.9 shock today. Thus, these potentially lethal faults need better understanding of their slip rate and earthquake history.

1. Introduction

[2] The 21 May 2003 M_w = 6.9 Zemmouri earthquake struck on a south dipping thrust fault whose surface trace is inferred to lie about 5–10 km offshore. The earthquake caused up to 0.8 m of coastal uplift and up to 0.24 m of horizontal displacement as measured by GPS. The earthquake source has been extensively investigated to identify the fault geometry and slip distribution using seismic, geodetic and coastal uplift data [*Meghraoui et al.*, 2004; *Yelles et al.*, 2004; *Delouis et al.*, 2004; *Semmane et al.*, 2005; *Braunmiller and Bernardi*, 2005; *Belabbes et al.*, 2009].

Studies were also carried out to investigate the relationship of the Zemmouri quake to the coastal tectonics of the Algerian fold and thrust belt [*Meghraoui et al.*, 2004; *Déverchère et al.*, 2005].

[3] The tectonics of northern Algeria is characterized by a series of en echelon thrust faults (Figure 1), which together accommodate 5–6 mm/yr of northwestward motion of Africa (Nubia) with respect to Eurasia [*Morel and Meghraoui*, 1996; *Nocquet and Calais*, 2004]. This is similar in geometry and rate to the well-studied continental thrust faults in central California, for example, Coalinga, Kettleman Hills [*Namson and Davis*, 1988; *Dickinson*, 2002; *Lin and Stein*, 2004], but significantly different from subduction zones, where thrust segments are much more continuous along strike [e.g., *Ando*, 1975; *Chlieh et al.*, 2004; *Subarya et al.*, 2006].

[4] The 2003 Zemmouri earthquake occurred on a system of highly segmented en echelon ruptures in the intraplate crust (Figures 1 and 2c). Thrust faults are linked by strike-slip faults into fault networks, the networks evolving into roughly perpendicular fault elements as the belt contracts and the faults mature. The historical and instrumental seismicity records reveal that the Boumerdes-Larbaa-Blida and

[1]Department of Geology and Geophysics, Woods Hole Oceanographic Institution, Woods Hole, Massachusetts, USA.
[2]U.S. Geological Survey, Menlo Park, California, USA.
[3]Institut de Physique du Globe de Strasbourg, EOST, Strasbourg, France.
[4]Disaster Prevention Research Institute, Kyoto University, Kyoto, Japan.
[5]Centre de Recherche en Astronomie Astrophysique et Geophysique, Algiers, Algeria.
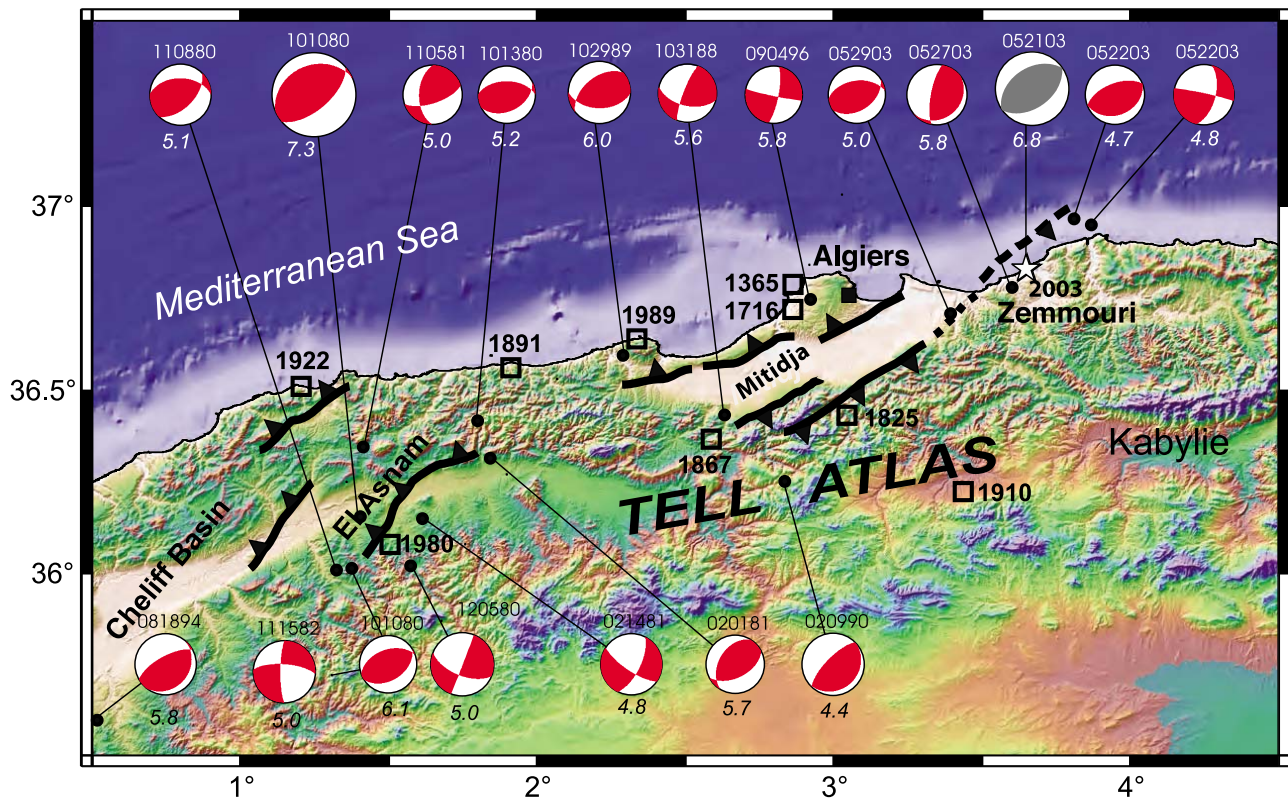[6]Now at SERTIT, Strasbourg, France.

Figure 1. The contractional tectonics of northern Algeria is characterized by a series of en echelon thrust faults of moderate lengths, on which about 30 $M \geq 5.5$ earthquakes have struck since records were kept beginning in about A.D. 1365 (modified from *Meghraoui et al.* [2004]). Notable among these are the highly destructive 1980 $M_w = 7.3$ El Asnam shock, as well as A.D. 1365 and 1716 earthquakes possibly located near Algiers [*Rothé*, 1950; *Benouar*, 1994]. The 19 largest global centroid moment tensor mechanisms are also shown, many of which are associated with the El Asnam event. The topographic expression of the thrust system is evident, but the role of offshore thrusts faults is less clear. The Mitidja basin in northern Algeria is bounded by the Boumerdes-Larbaa-Blida thrust fault system on the south and the Thenia strike-slip and Sahel thrust fault system on the north; these thrust systems have opposing dips [*Meghraoui*, 1988].

Sahel thrust fault systems are currently active, as both appear to exhibit seismicity during the historical (Figure 2a) and instrumental periods (Figures 2b and 2c). The record of strong quakes in the Mitidja basin (Figure 2a) likely reflects amplified basin shaking associated with earthquakes on either of the bounding thrust systems. During the most recent period, local network seismicity is evident on both thrust systems (Figure 2c).

[5] A large number of recent studies have investigated earthquake interaction in a variety of tectonic settings [e.g., *Harris*, 1998; *Parsons*, 2002, *Freed*, 2005; *Steacy et al.*, 2005]. Increasing evidence points to the importance of stress interaction among continental thrust events [e.g., *Harris et al.*, 1995; *Deng and Sykes*, 1997; *Hardebeck et al.*, 1998; *Wang and Chen*, 2001; *Wang et al.*, 2003; *Lin and Stein*, 2004] and among subduction earthquakes [e.g., *Dmowska et al.*, 1988; *Taylor et al.*, 1998; *Parsons*, 2002: *McCloskey et al.*, 2005; *Nalbant et al.*, 2005; *Pollitz et al.*, 2006]. However, the detailed features of stress interaction of earthquakes on en echelon thrusts and adjacent tear faults, like the ones observed in Algeria, are still poorly understood.

[6] In this paper we first explain the basis for Coulomb stress change calculations. This is followed by an illustration of what we believe to be the essential features of stress interaction among earthquakes occurring on en echelon thrusts and adjacent tear faults. We then seek to validate, or at least build confidence in, the coseismic stress change calculations using the recorded aftershocks and geodetically inferred afterslip following the 2003 Zemmouri earthquake. Finally, we investigate the Zemmouri earthquake stress interaction with the faults in its immediate surroundings and discuss its implications on future seismic hazard of the region.

2. Coulomb Stress Change Calculation

[7] We introduce changes in Coulomb failure stress function caused by a main shock, ΔCFF,

$$\Delta \mathrm{CFF} = \Delta\tau + \mu(\Delta\sigma + \Delta p), \qquad (1)$$

where $\Delta\tau$ is the shear stress change on a given fault plane (positive in the sense of fault slip), $\Delta\sigma$ is the fault normal
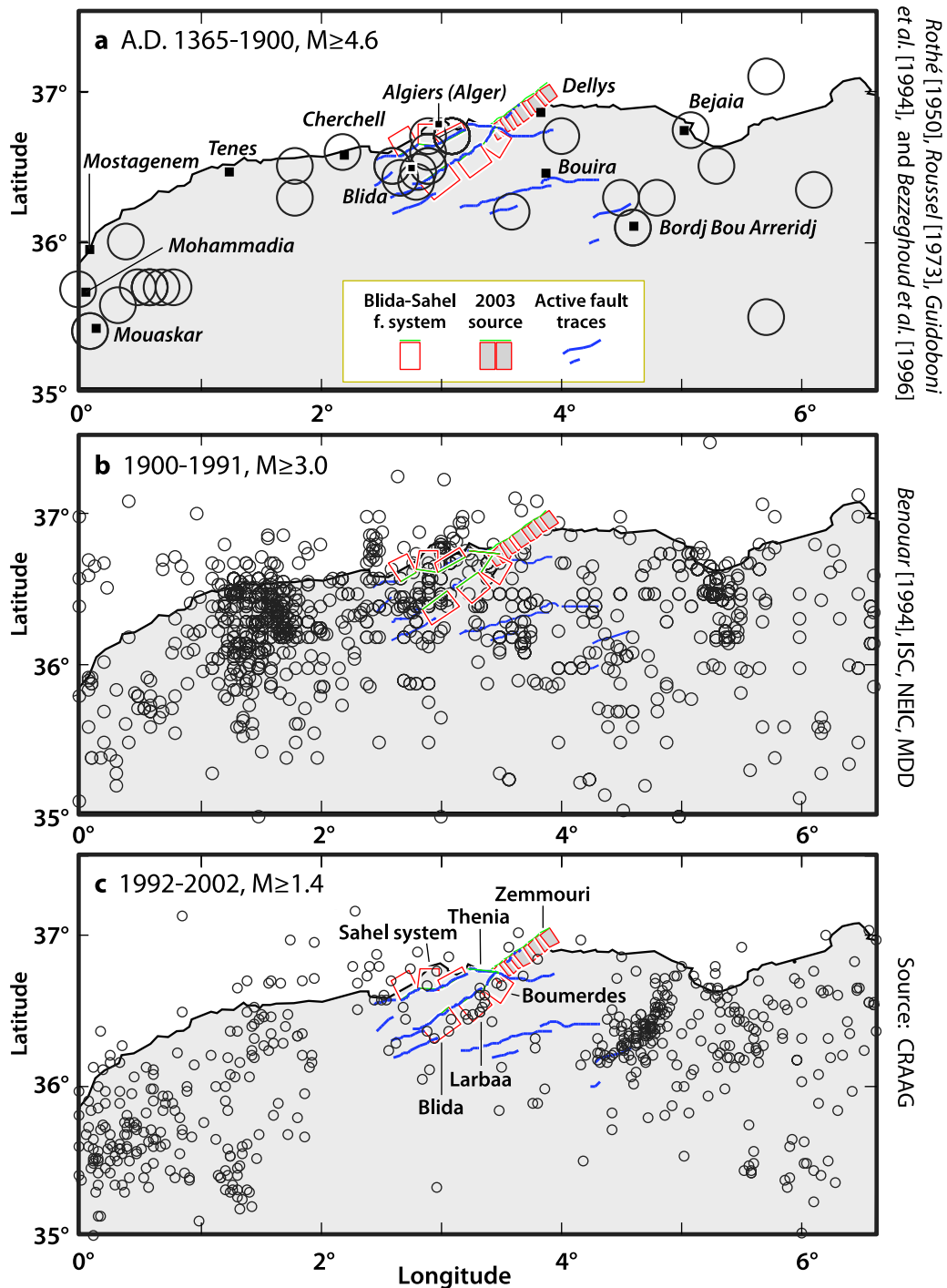
Figure 2. (a) Historical, (b) twentieth century, and (c) recent pre-Zemmouri seismicity in north central Algeria centered on the site of the 2003 earthquake [*Rothé*, 1950; *Roussel*, 1973; *Benouar*, 1994; *Guidoboni et al.*, 1994; *Bezzeghoud et al.*, 1996; *Ayadi et al.*, 2008]. Active faults are shown only within the greater Algiers region (36°N–37°N, 2.5°E–4.5°E) [*Meghraoui*, 1988]. Outside of the populated coastal region, location uncertainties are much larger and the completeness magnitude much greater than *M* = 5. The recent shocks (Figure 2c) were recorded by the Algerian national seismic network.
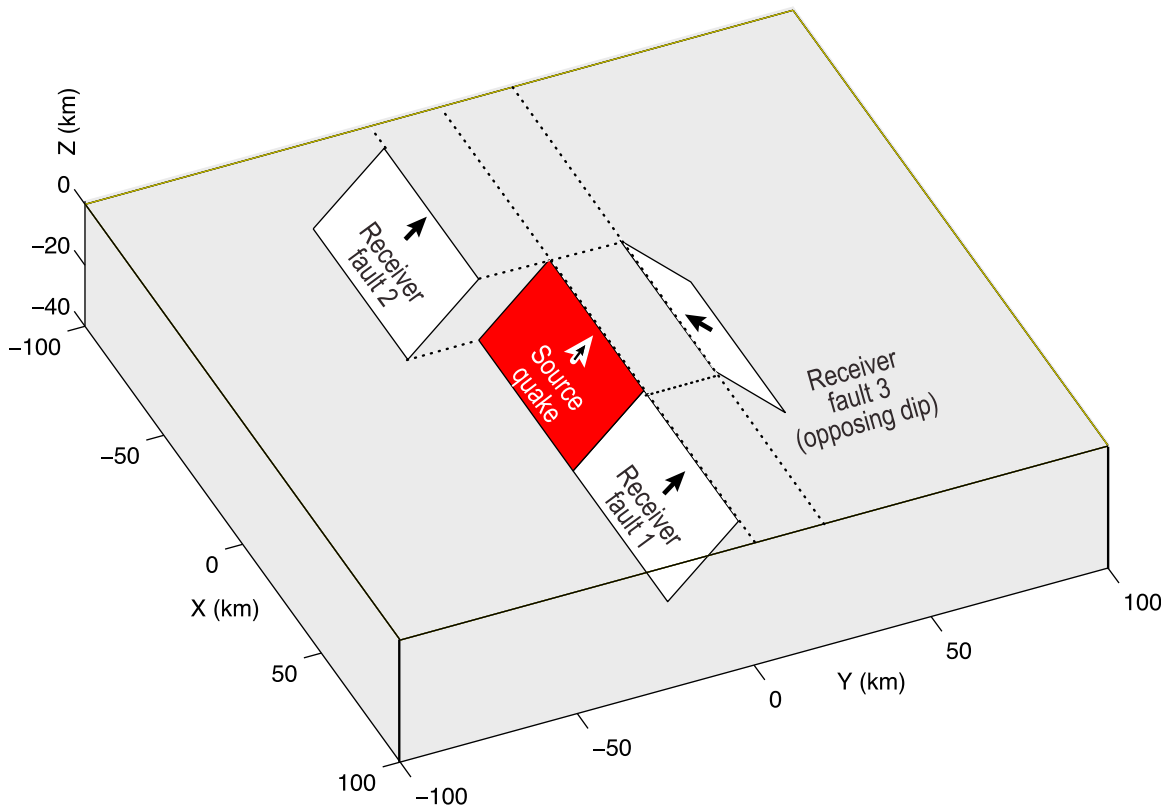
Figure 3. Schematic diagram showing a source thrust earthquake fault, an along-strike thrust receiver fault 1, an en echelon receiver fault 2, and receiver fault 3 with an opposing dip. We use the terms "source" to identify the fault that slipped seismically and "receiver" to indicate a fault on which we resolve the Coulomb stress imparted by the source. The average slip of the source earthquake is 1 m with rake of 90°; that is, pure thrust.

stress change (positive for fault unclamping), μ is the coefficient of friction, and Δp is the pore pressure change. Δp is generally poorly known but proportional to the changes in normal stress [*Ge and Stover*, 2000; *Cocco and Rice*, 2002], and so the majority of previous studies use the following simple expression, defining the apparent coefficient of friction μ' that implicitly includes the contribution of Δp:

$$\Delta\text{CFF} = \Delta\tau + \mu'\Delta\sigma. \qquad (2)$$

Stress tensors are computed from the simple Hook's law and coseismic strain tensors resolved in a homogeneous elastic half-space [*Okada*, 1992], in which the elastic body is governed by the shear modulus, which we assumed to be 3.2×10^5 bars, and Poisson's ratio, which we assumed to be 0.25. The coseismic shear stress caused by a "source" earthquake is resolved on specified planes of "receiver" faults, which are defined by their fault strike, dip, and rake. The normal stress change does not depend on the receiver fault rake. We used an apparent coefficient of friction, $\mu' = 0.4$ as a midrange value since μ' could range between 0.0 and about 0.8 [*King et al.*, 1994].

[8] We employ two types of visualization for the calculated ΔCFF. One is smoothed color-gradient maps of scalar values of ΔCFF resolved onto assumed uniform receiver planes defined by their strike, dip, and rake at gridded nodes at a given depth. These are used for examining the tendency of stress transfer for typical regional faults; we examine the spatial correlation between ΔCFF and aftershocks or seismicity rate changes. The other representation is a mosaic display of ΔCFF resolved onto patches of individual receiver faults, where color indicates the calculated ΔCFF at the center of each patch in the rake direction of each patch. These are used for estimation of the stress imparted to known or suspected faults in order to evaluate the potential interaction between the earthquake rupture and surrounding major faults. We approximated curved faults by a network of discrete fault patches; errors associated with such approximation decrease with decreasing sizes of the discrete fault patches. All calculations were carried out using the Coulomb 3.2 software (http://www.coulombstress.org).

2.1. Idealized Stress Transfer Among Thrust Faults

[9] Under what conditions can a thrust earthquake promote failure on surrounding faults? To answer this central question for earthquake interaction and seismic hazard in northern Algeria, we first analyzed a suite of idealized cases for $M = 7$ ruptures that reflect, in simplified form, the faulting configuration in Algeria.

[10] The simplest case is for a continuous planar fault with a thrust segment (receiver fault 1; see Figure 3) located
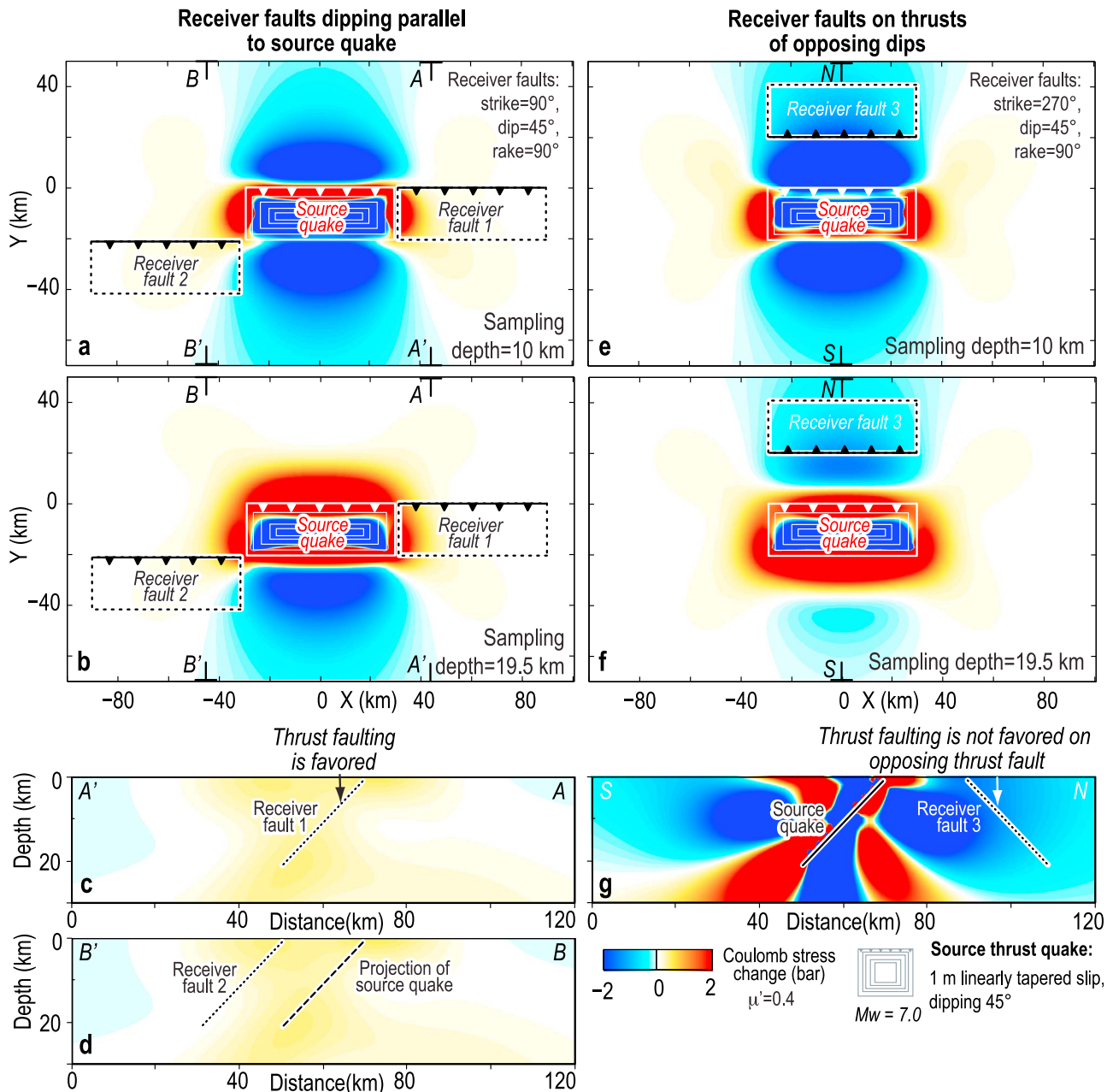
Figure 4. (a and b) Maps showing Coulomb stress changes caused by an $M = 7.0$ thrust earthquake on adjacent thrust faults either along strike (receiver fault 1) or en echelon (receiver fault 2). The 40 km long source quake has a tapered slip of 1 m, dips 45°, and ruptures from the ground surface to a depth of 20 km. Receiver faults have the same strike, dip, and rake as the source quake and at depth of 10 km (Figure 4a) and 19.5 km (Figure 4b). Cross sections at 10 km from the end of the source quake (cross section position shown in Figure 4a) are shown along profiles (c) A-A′ and (d) B-B′. Note that pure thrust faulting is favored over a wide zone beyond the end of a pure thrust quake. (e and f) Similar to Figures 4a and 4b, except that receivers have opposing dip. (g) Cross section along profile N-S through the midpoint of the source fault.

adjacent to a central pure thrust rupture (source quake; see Figure 3). We calculated Coulomb stress changes caused by the source quake on parallel thrust receiver faults (Figure 4). We tapered the source slip toward the edges of the rupture to minimize stress discontinuities at the rupture edges. One can see from Figures 4a–4c that an along-strike thrust fault (receiver fault 1) is brought closer to failure by the adjacent

rupture, but that the stress falls off quickly at distances greater than about one source width, regardless of the length of the source rupture. The result is symmetrical; the stress increase is the same on either side along strike of the source fault.

[11] The second case we considered is for echelon thrust faults (receiver fault 2; see Figure 3). The stress transfer is
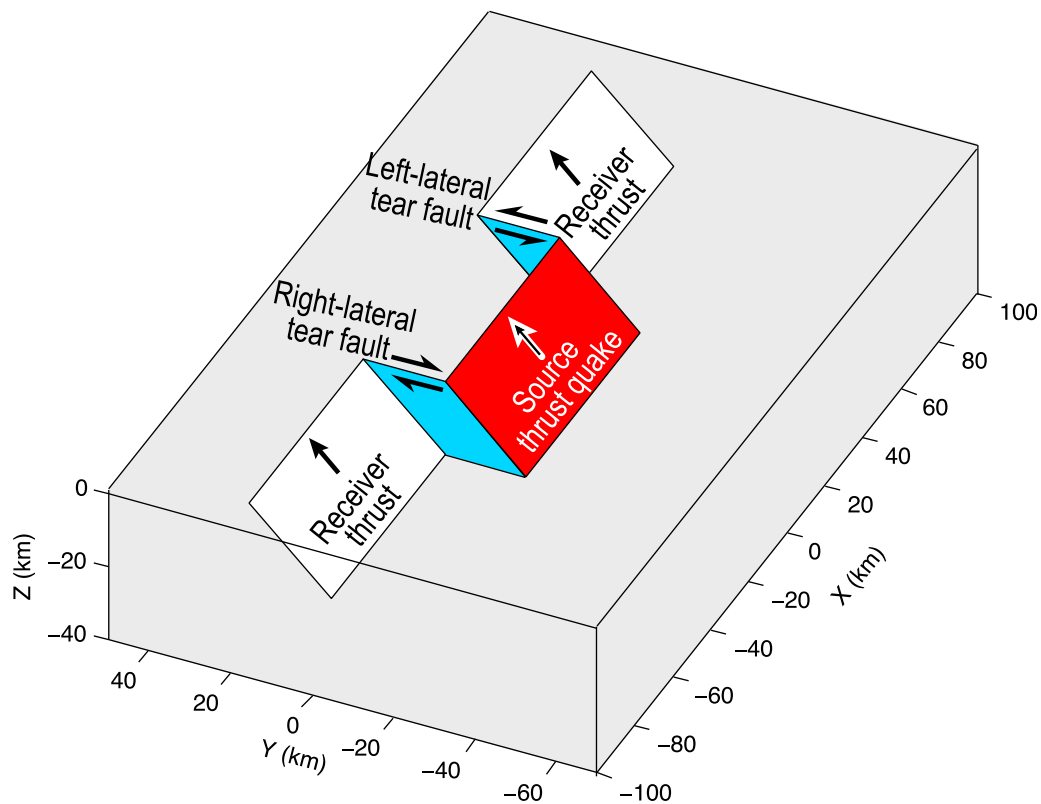
Figure 5. Schematic diagram showing right- and left-lateral tear faults connecting a source thrust earthquake fault and en echelon thrust receiver faults. The average slip of the source earthquake is 1 m with rake of 90°; that is, pure thrust.

illustrated to the left of the source fault in Figures 4a and 4b and in cross section in Figure 4d. Like the along-strike thrust fault, the en echelon thrust (receiver fault 2) is also brought closer to failure, but the stress increase diminishes roughly to zero at the base of the fault. Thus one might expect triggered earthquakes to preferentially nucleate at shallower depths.

[12] The third case is for opposing thrust faults on each side of a down-dropped basin (receiver fault 3; see Figure 3), resembling the structure of the Mitidja basin (Figure 1). Here, an earthquake on one thrust inhibits failure on the second (Figures 4e–4g). This inhibition is much stronger than the promotion in the former cases, and occurs regardless of the assumed value of friction. Thus rupture of one thrust fault locks the thrust across the basin, and so no triggering on an opposing thrust fault would be expected.

2.2. Idealized Stress Transfer Between Thrust and Tear Faults

[13] Tear faults or near-vertical shear zones likely connect en echelon thrusts at depth, as illustrated schematically in Figure 5. We calculated Coulomb stress changes caused by the source thrust quake on vertical tear faults that are orthogonal to the strike of the source fault (Figure 6). We find that slip on tear faults is strongly promoted by an adjacent thrust earthquake (Figure 6). Even though we tapered the source slip toward the edges of the rupture, the Coulomb stress increase on the tear faults is much larger

than it is for adjacent thrust faults (to appreciate this, compare the areas of stress increase in Figures 4 and 6). The near-surface stress change (see Figures 6a and 6e) may be large enough that surface slip might also be promoted. The imparted stress decreases with depth. Since the peak stress on the tear faults is just inboard of the edge of the thrust rupture, tear faults linking en echelon thrust sources would be strongly promoted.

[14] Our static stress calculations also show that when the thrust source has oblique slip, the tear faults are still favored. However, the stress imparted to the right-lateral tear fault is higher if the source has a right-lateral component, with the same for left-lateral source slip and left-lateral tears. In addition to the direct stress transfer from the thrust to tear faults as shown in Figure 6, *Magistrale and Day* [1999] illustrated that the presence of a tear fault favors the jump of dynamic rupture from the source earthquake fault to its adjacent thrust segments.

3. Consistency Tests of the 2003 Zemmouri Stress Transfer Calculations

[15] Next we seek to test whether the calculated coseismic stress changes are reflected in observations of postseismic fault slip and seismicity of the 2003 Zemmouri earthquake. We first assessed whether the reported afterslip on the shallow part of the 2003 source is consistent with the coseismic static stress changes caused by the Zemmouri earthquake.
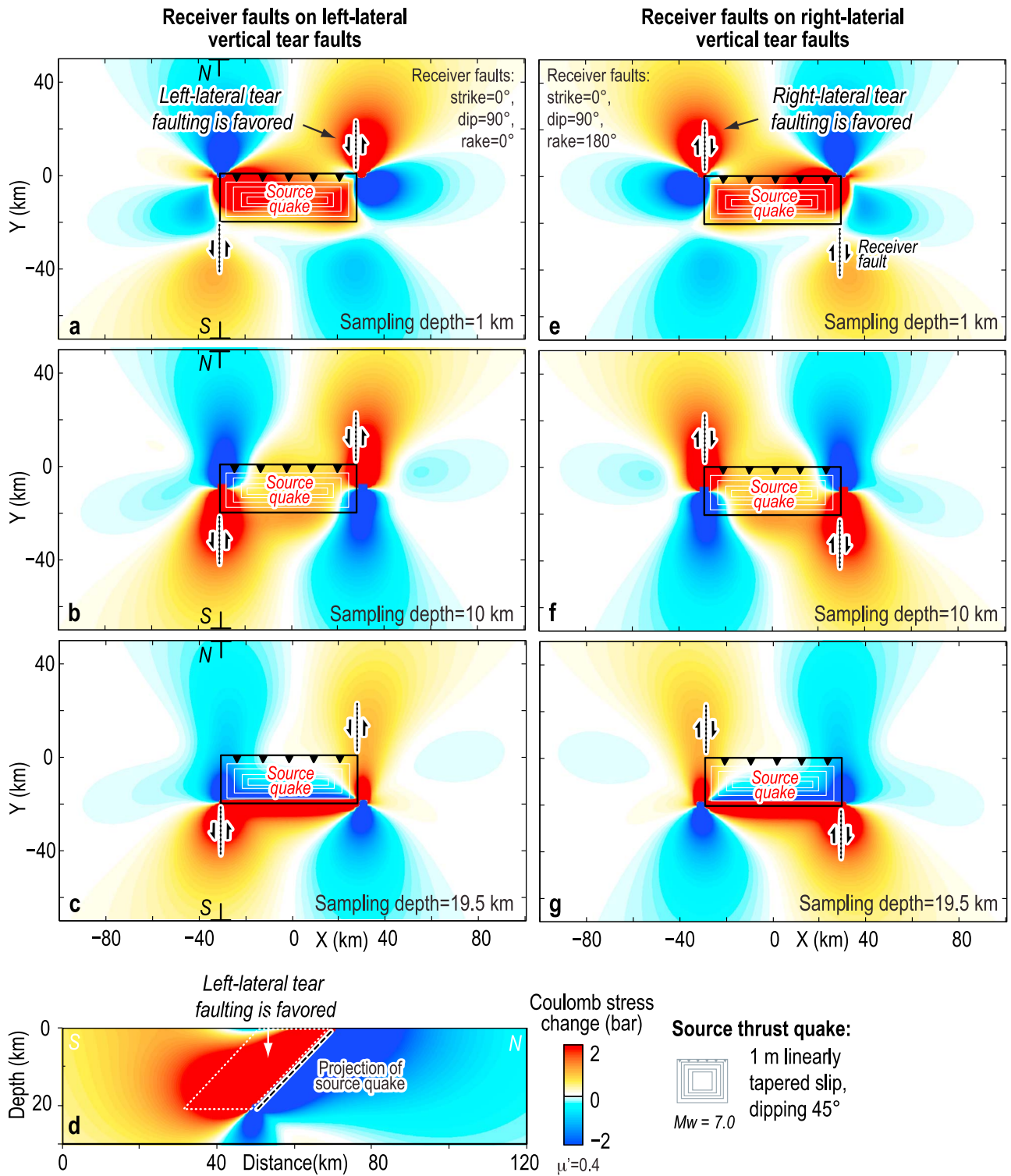
Figure 6. Maps showing Coulomb stress changes caused by an $M = 7.0$ earthquake on adjacent tear faults. The source is the same as in Figure 4. Coulomb stresses are calculated on (a–c) left-lateral and (e–g) right-lateral tear faults. Stress is sampled at depth of 1 km (Figures 6a and 6e), 10 km (Figures 6b and 6f), and 19.5 km (Figures 6c and 6g). (d) Cross section at the right end of the source earthquake (cross section position shown in Figure 6a). Note that left-lateral tear faulting is favored in one position with respect to the thrust, while right-lateral faulting is favored in the opposite position.
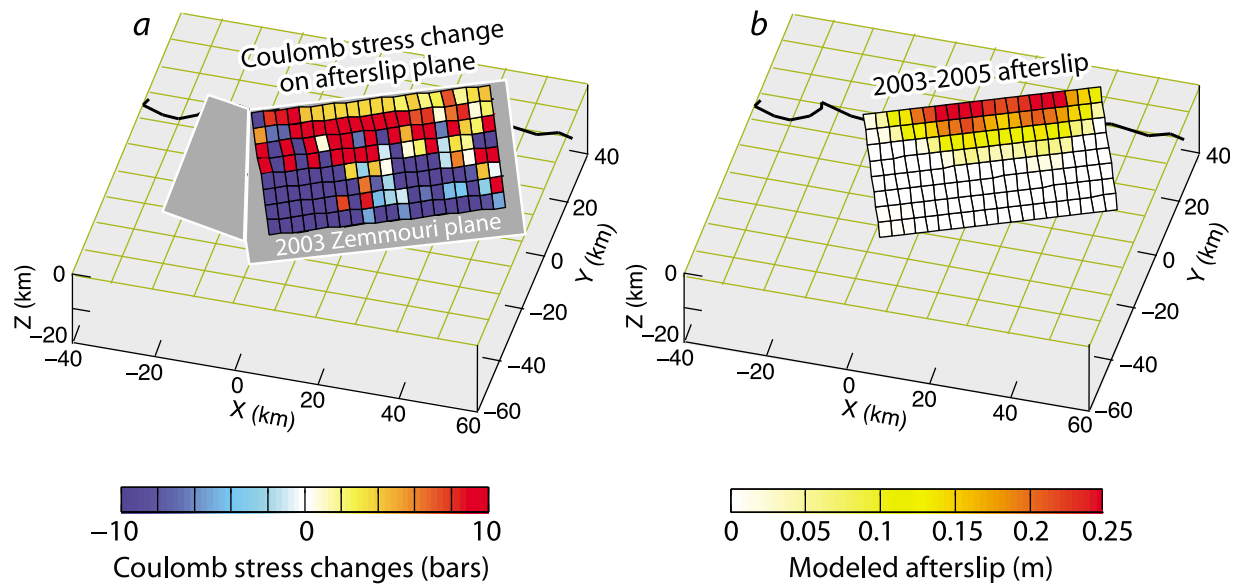
Figure 7. (a) Calculated Coulomb stress changes on the fault plane based on the *Belabbes et al.* [2009] source model. Patches of calculated Coulomb stress increase of 4–25 bars tend to occur at the shallowest 5–10 km of the fault. The stress changes on the western fault segment (left gray patch) of the *Belabbes et al.* [2009] source are <0.2 bar. (b) Afterslip during 2003–2005 from *Mahsas et al.* [2008]. Note that the afterslip is concentrated where the coseismic stress increases are high.

We then examined the well-located aftershocks and their focal mechanisms to see if the calculated Coulomb stresses are consistent with the promotion of fault slip on their nodal planes. While these tests are inevitably insufficient to validate the stress calculations in a strict sense, if the observations were inconsistent with the model, they could invalidate the calculations.

3.1. Zemmouri Rupture Model

[16] For the Zemmouri earthquake, several variable slip models have been inverted from the seismic and geodetic data to constrain the coseismic rupture geometry [*Meghraoui et al.*, 2004; *Delouis et al.*, 2004; *Semmane et al.*, 2005; *Braunmiller and Bernardi*, 2005]. Most recently, *Belabbes et al.* [2009] jointly inverted the coastal uplift, GPS and InSAR data. Here we used the simpler ten patch model by *Meghraoui et al.* [2004] and the variable slip model by *Belabbes et al.* [2009], which benefits from the use of InSAR data. But we modestly simplified the curved surface of the *Belabbes et al.* [2009] model with two rectangular patches, each with variable slip. The 65 km long main rectangle strikes 60° and the smaller 13 km long southwest rectangle strikes 102°; both dip 45° to the southeast and undergo pure dip slip.

[17] From the inversion of surface deformation data obtained from InSAR, GPS, and coastal uplift measurements, *Belabbes et al.* [2009] provided a source model with seismic moment of 2.15×10^{26} dyne cm. We have slightly rescaled their model so that it yields $M_w = 6.9$ (2.3×10^{26} dyne cm), which represents the most commonly inferred size of this earthquake by all other studies; *Semmane et al.* [2005] find $M_w = 7.1$, and *Delouis et al.* [2004] and *Meghraoui et al.* [2004] find $M_w = 6.9$.

3.2. Stress Transfer and Afterslip

[18] *Mahsas et al.* [2008] used postseismic GPS observations to infer the distribution of postseismic slip. There is abundant evidence that postseismic creep is promoted by coseismic stress changes, typically updip and downdip of the seismic rupture [e.g., *Reilinger et al.*, 2000; *Hearn et al.*, 2002; *Lin and Stein*, 2004]. For the Zemmouri earthquake, *Mahsas et al.* [2008] inverted six continuous GPS records from the epicentral area for the 2.5 years following the event. They argued that the data are poorly explained by viscoelastic relaxation, or by poroelastic rebound, and that instead the concentration of afterslip adjacent to and updip of the coseismic rupture is more consistent with being driven by coseismic stresses.

[19] We used the *Belabbes et al.* [2009] source model to calculate the Coulomb stress change on the source plane (Figure 7a). The blue regions below 10 km generally depict large stress drops, whereas the majority of the upper 5–10 km display stress increases of 1–20 bars. These increases correlate with the sites of modeled afterslip (Figure 7b). The correlation is best seen in a plot of modeled afterslip as a function of calculated coseismic stress change (Figure 8). Some 125 patches or 78% of the total have positive correlation between afterslip and Coulomb stress change (red and gray dots), and 35 do not (blue and white dots). A similar correlation between coseismic stress and afterslip was found for the 1999 $M = 7.6$ Chi-Chi earthquake by *Chan and Stein* [2009]. Simply put, the afterslip occurred on the updip extension of the coseismic slip surface, where most of the high afterslip patches were calculated to have Coulomb stress increase of less than 20 bars (Figure 8).
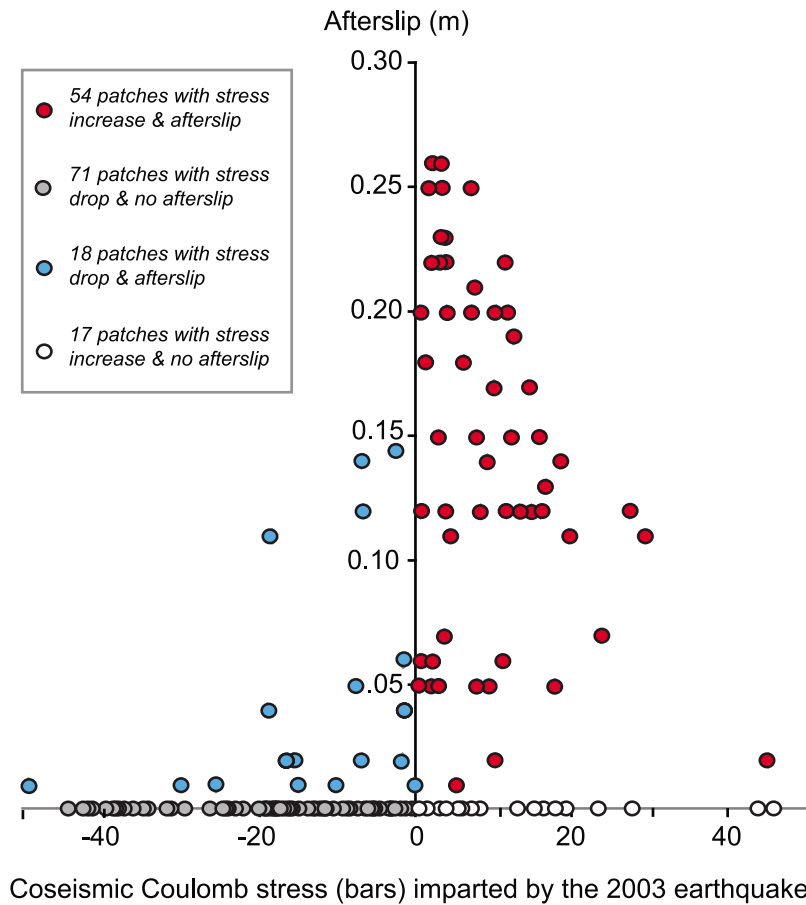
Figure 8. Comparison between the calculated Coulomb stress changes using the *Belabbes et al.* [2009] source model and afterslip from *Mahsas et al.* [2008] on 160 patches that define the afterslip surface. Among the patches with afterslip, 54 are associated with a calculated stress increase while 18 patches with a stress drop, suggesting that afterslip was at least in part triggered by the coseismic stress changes.

3.3. Consistency With Mechanism of Aftershocks

[20] If the Coulomb stress increase promoted the aftershock failure, one would expect to see that faulting mechanisms of aftershocks should correlate with the coseismic Coulomb stress increase [*Hardebeck et al.*, 1998]. *Ayadi et al.* [2008] relocated Zemmouri aftershocks in a 3D velocity model using a double-difference method and calculated focal mechanisms for 30 aftershocks during 1–27 June 2003 (Figure 9), which occurred throughout the rupture area. Except for the special case of zero fault friction, the Coulomb stress imparted to the two nodal planes will be different, and we do not know which of the two planes slipped. Therefore we resolve the coseismic Coulomb stress change on both nodal planes of each of these mechanisms, and plot the resulting stress changes in Figure 10.

[21] The Coulomb stress change is positive for at least one nodal plane in 27 (90%) out of 30 aftershocks and positive for both nodal planes of 23 aftershocks (77%), while the shear stress change is positive for 20 out of 30 aftershocks (67%). The mean Coulomb stress change averaged for both nodal planes is about 2 bars. A positive correlation of stress transferred to aftershock focal planes was also found for the 1992 M_w = 7.3 Landers [*Hardebeck et al.*, 1998; *Seeber and Armbruster*, 2000] and 1999 M_w = 7.6 Chi-Chi [*Ma et al.*, 2005] aftershocks. Those cases benefited from an extensive pre–main shock focal mechanism catalog, allowing them to calculate the gain in post–main shock Coulomb correlation over the pre–main shock correlation, a stronger test of the triggering hypothesis than what we can conduct here. Unfortunately, in the 1.5° latitude by 2.5° longitude area centered on the 2003 Zemmouri main shock, there are only 6 global centroid moment tensor (CMT) catalog solutions, and none of these strike in the area of the 2003 aftershocks, precluding such a test.

3.4. Long-Term Activation of Off-Fault Seismicity Triggered by the Zemmouri Shock

[22] The internal consistency tests we have presented increase our confidence in the calculated coseismic stress changes for the 2003 Zemmouri rupture, and thus encourage their use in assessing the changes in seismic hazard imposed by the earthquake.

[23] Over the 7 years since the 2003 main shock, the entire south dipping thrust system extending 80 km to the southwest experienced an increased rate of seismicity (Figure 11). Relative to the period before the 2003 main
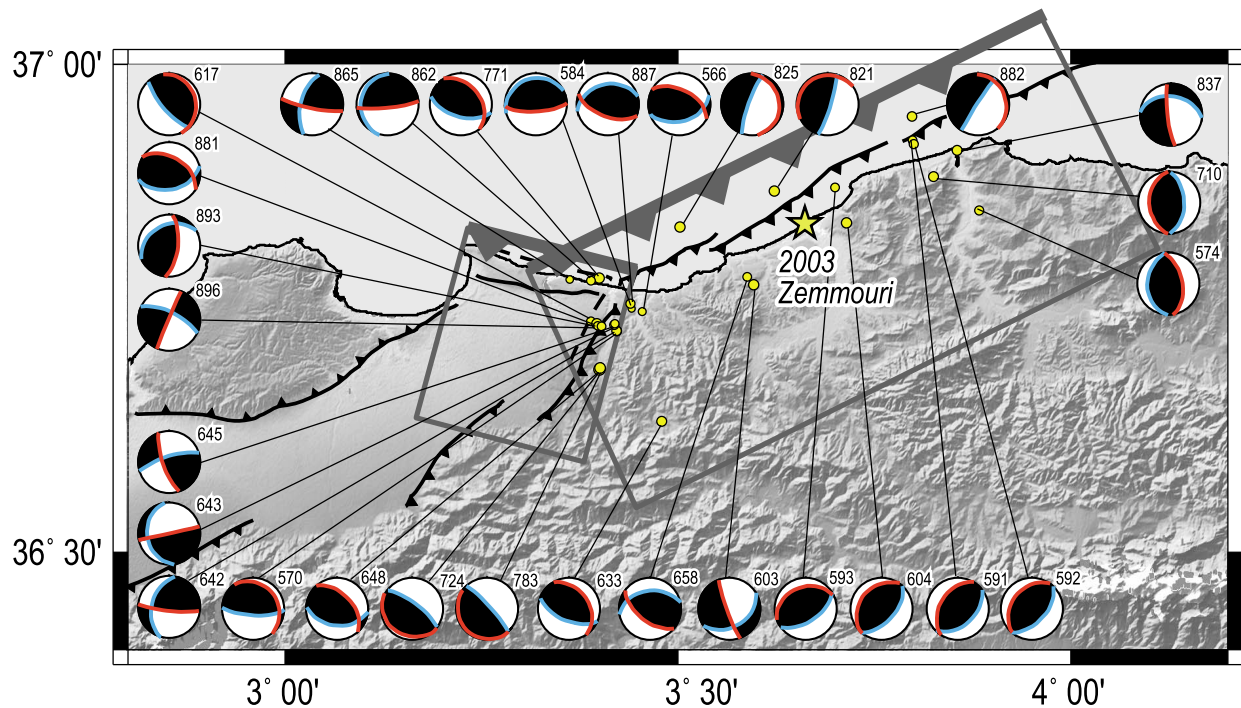
Figure 9. Thirty relocated aftershocks with focal mechanisms from *Ayadi et al.* [2008] were used in the stress transfer analysis together with the *Belabbes et al.* [2009] source planes. The nodal planes inscribed in red are arbitrarily identified as plane 1, and blue as plane 2, in Figure 10.
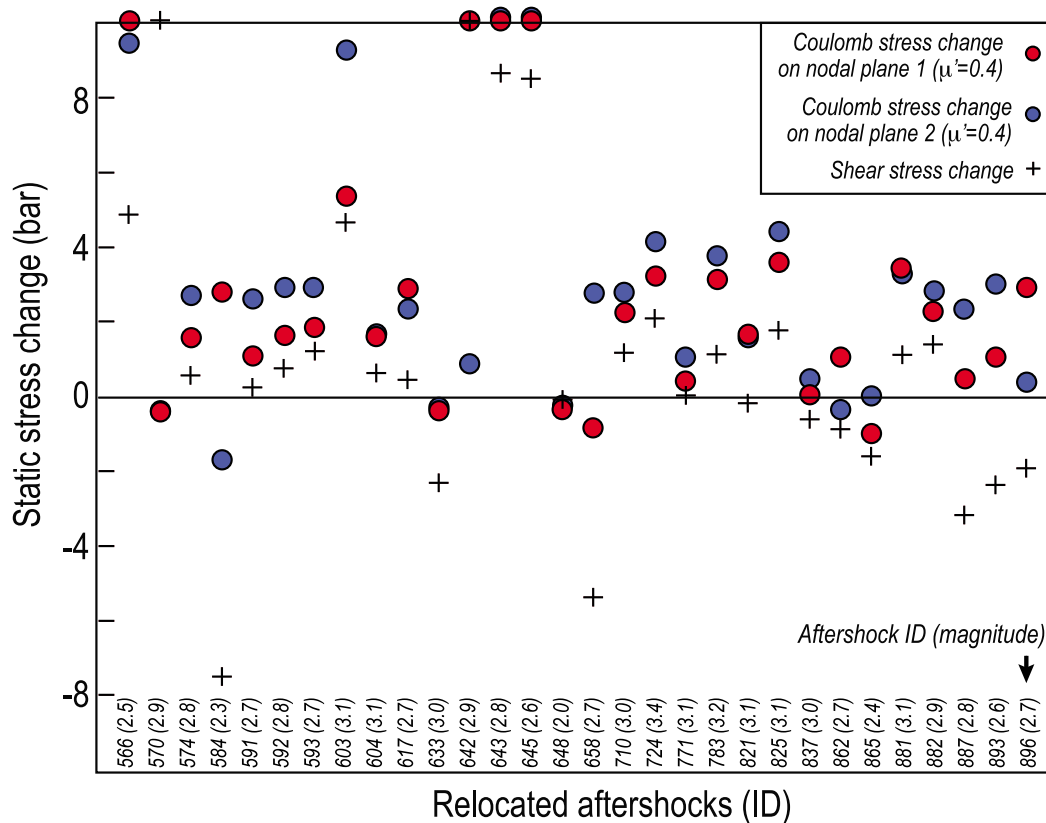

Figure 10. Calculated stress changes caused by the 2003 Zemmouri earthquake on nodal planes of relocated aftershocks from *Ayadi et al.* [2008]. Stress calculations were made using the *Belabbes et al.* [2009] source. The values plotted along the upper frame exceed 10 bars. Note that the majority of the nodal planes were calculated to have experienced stress increase caused by the main shock.
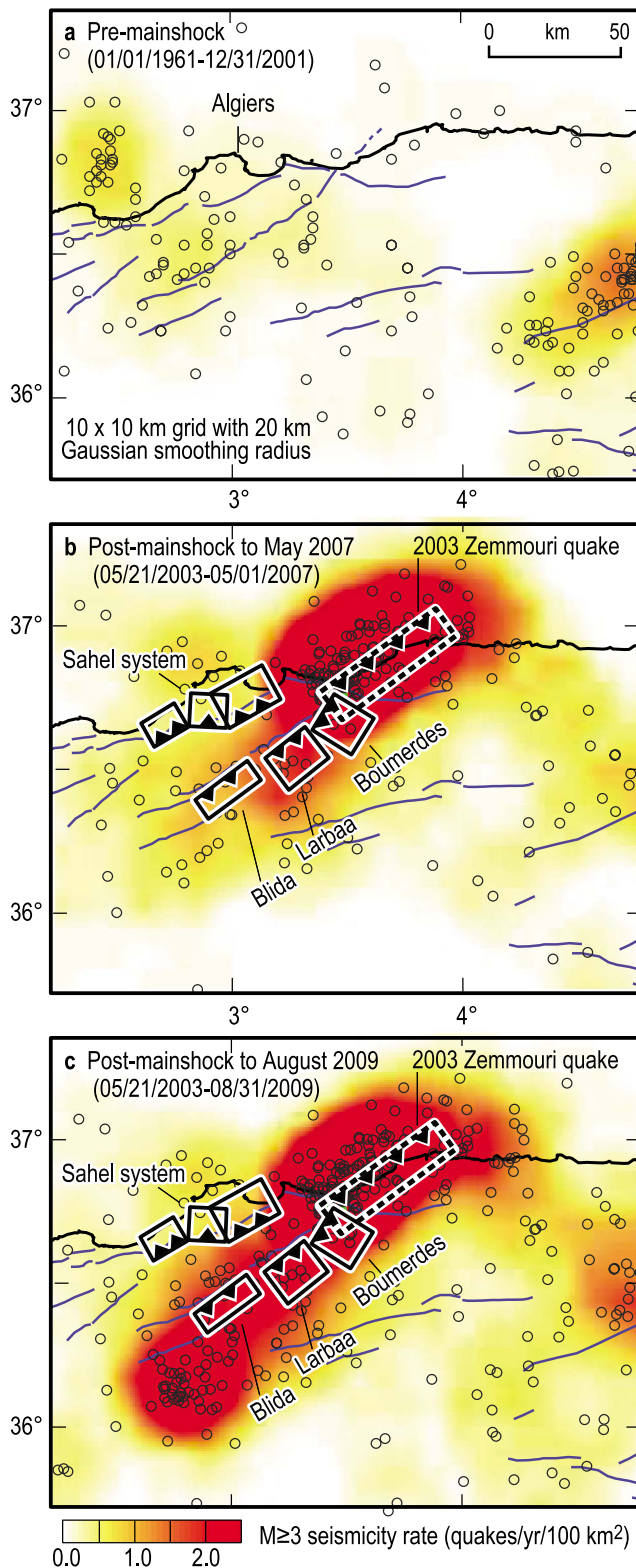
Figure 11. (a) Seismicity rate before the Zemmouri earthquake, (b) post–main shock to May 2007, and (c) post–main shock to August 2009. In 2003–2007 the rate increases not only near the 2003 rupture, but also along the Boumerdes and Larbaa segments (Figure 11b). After an $M = 5.2$ quake southwest of Blida in 2007, the rate increase extends the entire south dipping thrust system (Figure 11c).

shock (Figure 11a), the Boumerdes and Larbaa faults undergo post–main shock seismicity rate increases in 2003–2007 (Figure 11b). An $M = 5.2$ shock occurred southwest of the Blida thrust on 22 August 2007. During the next 2 years all 3 thrusts sustained a higher rate of seismicity than occurred before the 2003 Zemmouri main shock (Figure 11c).

4. Stress Changes Caused by the 2003 Zemmouri Earthquake

4.1. Stress Transferred to the Surrounding Crust

[24] In Figure 12, we furnish a calculation of the stress transfer field at a midcrustal depth under the simplifying assumption that all receiver faults have a geometry either resembling the ensemble Boumerdes, Larbaa, and Blida thrust system (Figures 12a and 12b), or the Sahel system (Figures 12d–12e). Although the *Meghraoui et al.* [2004] and *Belabbes et al.* [2009] coseismic slip models yield a similar stress distribution, their most important difference is the greater stress transfer to the east Sahel fault, which underlies the city of Algiers (Figure 12). Figures 12a and 12b can be compared to the idealized case in Figures 4a and 4b for en echelon thrusts with the same dip; whereas Figures 12d–12e can be compared to Figures 4e and 4f for thrusts of opposing dip. Despite the complexity of the variable slip models used in Figure 12, it is evident that the principal features of stress transfer can be seen in the simpler tapered slip faults as long as they have about the same seismic moment.

4.2. Stress Transferred to the Boumerdes-Larbaa-Blida, Thenia, and Sahel Fault Systems

[25] We next calculated the Coulomb stress resolved on the Boumerdes-Larbaa-Blida thrust faults bounding the southern margin of the Mitidja basin, and find that the western portion of the Boumerdes thrust, and to a lesser extent, the eastern portion of the Larbaa thrust, were brought closer to Coulomb failure by the Zemmouri earthquake (Figure 13). The Boumerdes stress is calculated to have increased by up to 1.5 bars, with the Larbaa increased by up to 0.4 bar. The Zemmouri stress promotes slip on the strike-slip Thenia fault by >2 bars in the upper 5–8 km, but inhibits slip by >2 bars below 8–10 km (Figure 13, inset). We calculated that the east section of the Sahel fault was brought up to 0.4 bar closer to failure, with negligible stress changes on faults farther west of the Zemmouri rupture surface (Figure 13). The first 2 years of shallow afterslip only slightly increases the stress on the Boumerdes and Larbaa faults (Figure 12c); the same is true for the Thenia and east Sahel fault.

5. Discussion

5.1. Generalizing Zemmouri to Thrust Fault Interactions

[26] The interactions among simple thrusts and tear faults presented in an early section of the paper shed light on the Zemmouri earthquake triggering. We showed that a thrust fault brings en echelon thrusts closer to failure (Figures 4a–4d), and this is seen for the Boumerdes thrust (Figures 12a and 12b). The Boumerdes thrust sustains a calculated stress increase and is at least partially bathed in aftershocks
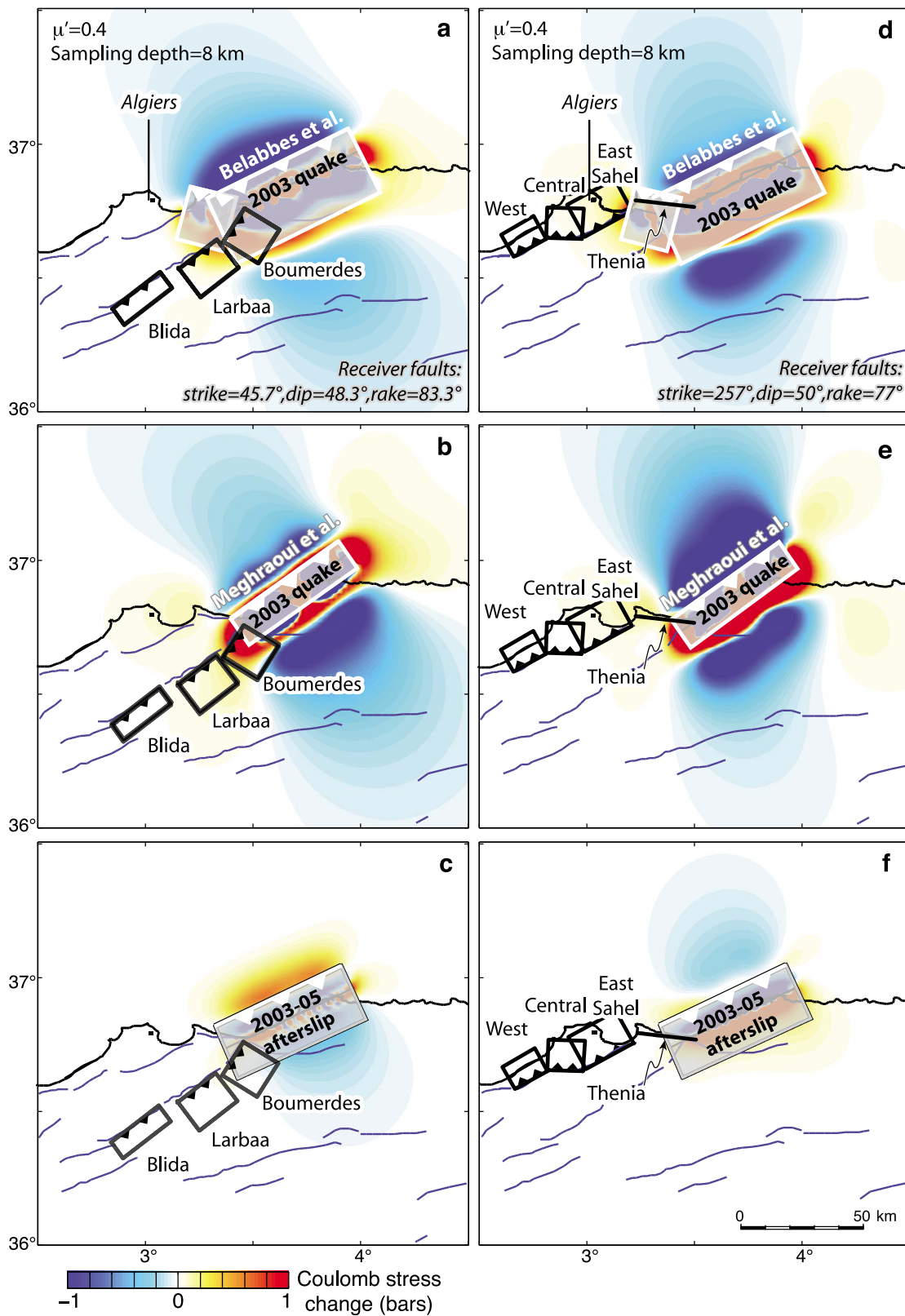
Figure 12. Calculated Coulomb stress changes at depth of 8 km along (a–c) the Boumerdes, Larbaa, and Blida faults and (d–f) the Thenia-Sahel faults. The receiver faults were assumed to have average fault parameters of their systems (Boumerdes, Larbaa, and Blida in Figures 12a–12c with strike/dip/rake = 45.7°/48.3°/83.3°; Sahel in Figures 12d–12f, strike/dip/rake = 257°/50°/77°). The coseismic source models of *Belabbes et al.* [2009] (Figures 12a and 12d) and *Meghraoui et al.* [2004] (Figures 12b and 12e) were both used, as well the afterslip model [*Mahsas et al.*, 2008] (Figures 12c and 12f).
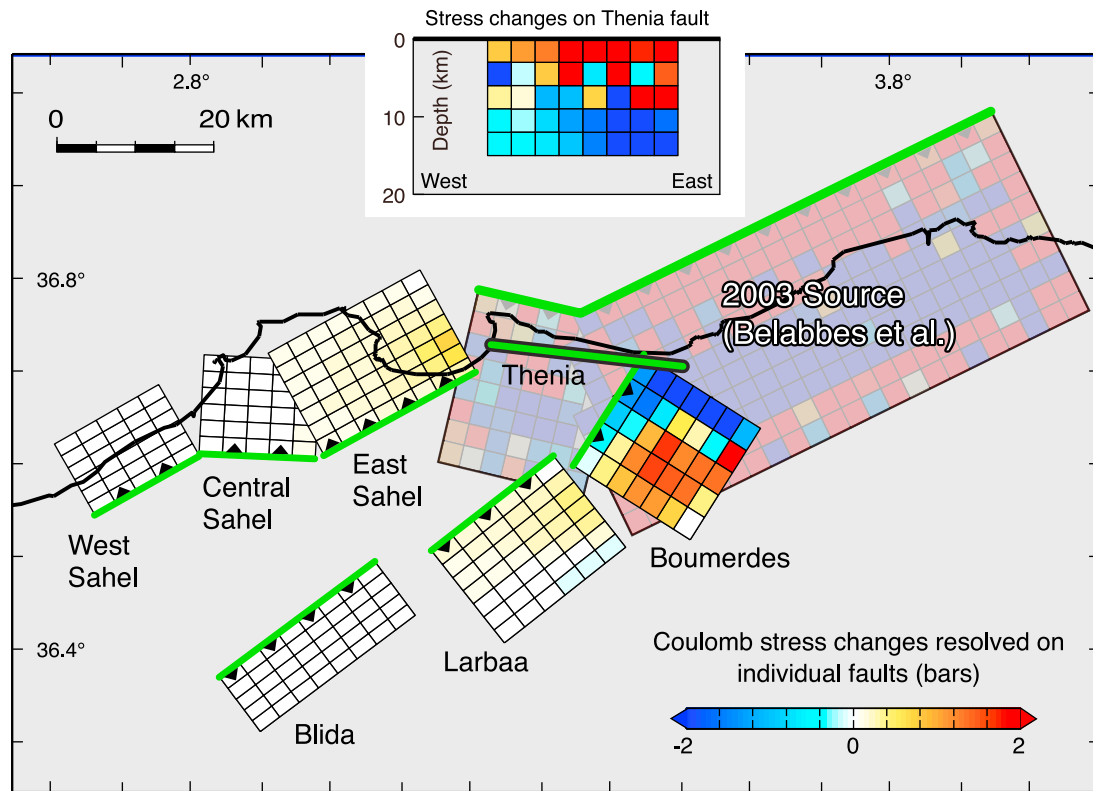
Figure 13. Calculated Coulomb stress changes caused by the 2003 Zemmouri earthquake resolved on the Boumerdes, Larbaa, and Blida fault segments and the Sahel fault system based on the Zemmouri slip model of *Belabbes et al.* [2009]. The assumed dip/rake of the faults were as follows: Boumerdes (40°/90°), Larbaa (45°/80°), Blida (60°/80°), Thenia (90°/180°; shown as an inset), Sahel east (45°/70°), central (45°/70°), and west (45°/70°). All faults were assumed to extend to 15 km depth.

(Figure 14). We also showed that slip at depth on a tear fault with the correct sense of slip is strongly promoted (Figure 6); this is similar to the Thenia fault, which is the site of triggered slip at depth [*Belabbes et al.*, 2009] and aftershocks (Figure 14). We also showed that parallel thrust faults located perpendicular to strike of the source quake are inhibited from failure, regardless of whether they dip in the same direction (Figures 4a and 4b) or opposite to the rupture Figures 4e–4g). *Déverchère et al.* [2005] found morphological evidence for active thrust faults north of the Zemmouri fault in the bathymetry, but none of these faults were activated by the Zemmouri shock, consistent with this expectation.

5.2. Implications of Stress Transfer for Earthquake Hazard Changes

[27] An inverted Y-shaped aftershock distribution is evident to the southwest of the Zemmouri rupture surface, these off-fault aftershocks appear to encompass the stressed portions of the Thenia and Boummerdes faults (Figure 14). *Belabbes et al.* [2009] found coseismic offsets across the Thenia fault from InSAR data between Zemmouri and Cape Matifou, which they modeled by 0.15–0.38 m along 20 km of a right-lateral vertical Thenia fault, in a similar sense but longer than the 2–3 km of surface cracks observed in the

field. These observations are consistent with the shallow stress changes promoting right-lateral slip (Figure 13, inset).

[28] The Coulomb stress transfer calculations help guide our understanding of how the long-term seismic hazard has been altered by the Zemmouri earthquake. The most strongly stressed fault is the Boumerdes; its deeper western portion was subjected to a calculated 1–2 bar increase (Figure 13). The next most stressed fault is the Thenia, although only the shallower portions of the fault are brought 1–2 bars closer to failure; the deeper, presumably seismogenic portion was inhibited from failure (Figure 13, inset). The east Sahel and Larbaa thrusts are both brought up to 0.4 bar closer to failure (Figures 12 and 13). Unfortunately, we can say little about the east end of the 2003 rupture despite the large off-fault stresses; *Déverchère et al.* [2005] mapped en echelon thrusts east of the Zemmouri rupture, but background seismicity is quite low.

[29] While we can estimate the stress increases on these faults, it is much more difficult to assess how close the Boumerdes and east Sahel faults are to failure, since their long-term slip rate is unknown. Given the 5–6 mm/yr contraction rate, the Blida and Sahel systems could perhaps each have rates of ~2 mm/yr (see also discussion in the work of *Meghraoui and Doumaz* [1996]). The Sahel thrust might have ruptured in A.D. 1365 and 1716 (Figure 1), in which case the potential for about 0.6–1.3 m of slip now exists,
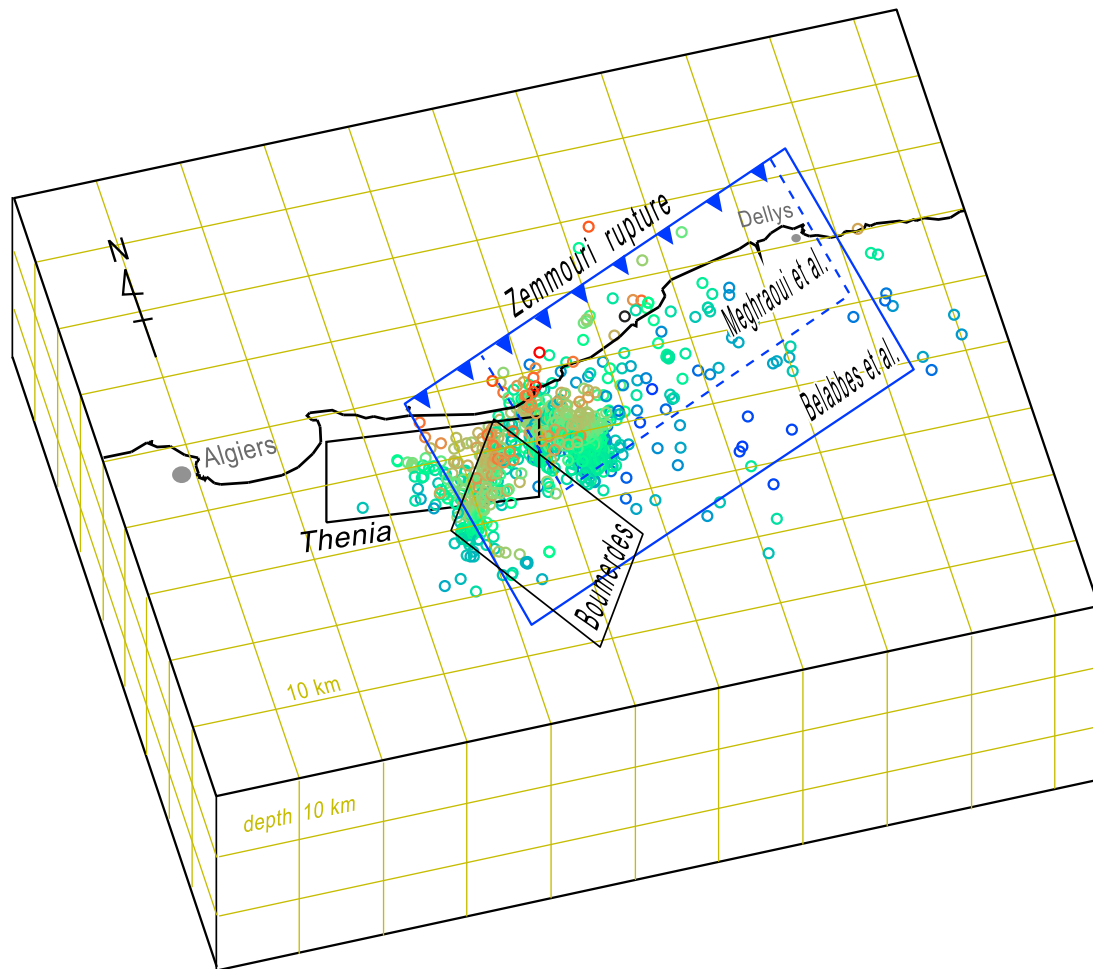
Figure 14. Perspective view of the first 2 months of Zemmouri aftershocks (1500 events) from *Ayadi et al.* [2008] together with the Thenia and Boumerdes faults, and both the *Meghraoui et al.* [2004] and *Belabbes et al.* [2009] rupture surfaces. Aftershocks appear to strike near both the Boumerdes and Thenia faults, which either overlap or lie just to the west of the main shock rupture. Aftershocks are colored by depth: red, 0–5 km; green, 5–10 km; and blue, >10 km.

equivalent to a minimum M_w = 6.6–6.9 earthquake considering the estimated fault surface area of the eastern section of the Sahel thrust system. Unless paleoseismic investigations can provide constraints on past earthquake parameters, the long-term hazard of the eastern Mitidja basin will remain even less clear. What is certain is that large ruptures on either the east Sahel or Boumerdes thrust would strongly affect Algiers; these faults pose the greatest seismic risk to the capital city, and need further seismotectonic investigations.

6. Conclusions

[30] We have shown that the 2003 Zemmouri earthquake transferred stress to several surrounding en echelon thrusts and at least one strike-slip tear fault. This process leads to off-fault aftershocks and could potentially to propagating earthquake sequences in the future. A variable slip model [*Belabbes et al.*, 2009] was used to calculate stress transferred to the sites of afterslip and aftershocks with focal mechanisms, and in both cases a high correlation was found with coseismic stress increases. We also calculated that the

shallower portions of the right-lateral Thenia fault were brought >2 bars closer to failure; InSAR data reveals about 0.15–0.38 m of likely coseismic offsets along the 20 km long fault.

[31] Bolstered by these internal tests of the Coulomb stress calculations, we found that the 2003 Zemmouri quake brought the deeper and western portion of Boumerdes thrust up to 1.5 bars closer to failure, and the east Sahel and Larbaa thrusts up to 0.4 bar closer to failure. The calculated pattern of the stress increase on the Boumerdes fault appears at least roughly consistent with the 2003 Zemmouri aftershocks, which illuminated parts of the Boumerdes thrust. We regard the Boumerdes and east Sahel faults as the most threatening earthquake sources for Algiers, and thus, we advocate deeper study of their slip rate and past earthquake history.

References

Ando, M. (1975), Source mechanisms and tectonic significance of historical earthquakes along the Nankai Trough, Japan, *Tectonophysics*, *27*, 119–140, doi:10.1016/0040-1951(75)90102-X.

Ayadi, A., C. Dorbath, F. Ousadou, S. Maouche, M. Chikh, M. A. Bounif, and M. Meghraoui (2008), Zemmouri earthquake rupture zone (M_w 6.8, Algeria): Aftershocks sequence relocation and 3D velocity model, *J. Geophys. Res.*, *113*, B09301, doi:10.1029/2007JB005257.

Belabbes, S., C. Wicks, Z. Cakir, and M. Meghraoui (2009), Rupture parameters of the 2003 Zemmouri (M_w 6.8), Algeria, earthquake from joint inversion of interferometric synthetic aperture radar, coastal uplift, and GPS, *J. Geophys. Res.*, *114*, B03406, doi:10.1029/2008JB005912.

Benouar, D. (1994), The seismicity of Algeria and adjacent regions, *Ann. Geofis.*, *37*(4), 1–862.

Bezzeghoud, M., A. Ayadi, A. Sebaï, A. Messaoud, A. Mokrane, and H. Benhallou (1996), Seismicity of Algeria between 1365 and 1989: Map of maximum observed intensities (MOI), *Av. Geofis. Geod. 1*, pp. 107–114, Minist. de Obras, Transp. y Media Ambiente, IGN, Madrid.

Braunmiller, J., and F. Bernardi (2005), The 2003 Boumerdes, Algeria, earthquake: Regional moment tensor analysis, *Geophys. Res. Lett.*, *32*, L06305, doi:10.1029/2004GL022038.

Chan, C.-H., and R. S. Stein (2009), Stress evolution following the 1999 Chi-Chi, Taiwan, earthquake: Consequences for afterslip, relaxation, aftershocks, and departures from Omori decay, *Geophys. J. Int.*, *177*, 179–192, doi:10.1111/j.1365-246X.2008.04069.x.

Chlieh, M., J. B. de Chabalier, J. C. Ruegg, R. Armijo, R. Dmowska, J. Campos, and K. Feigl (2004), Crustal deformation and fault slip during the seismic cycle in the north Chile subduction zone, from GPS and InSAR observations, *Geophys. J. Int.*, *158*, 695–711, doi:10.1111/j.1365-246X.2004.02326.x.

Cocco, M., and J. R. Rice (2002), Pore pressure and poroelasticity effects in Coulomb stress analysis of earthquake interactions, *J. Geophys. Res.*, *107*(B2), 2030, doi:10.1029/2000JB000138.

Delouis, B., M. Vallee, M. Meghraoui, E. Calais, S. Maouche, K. Lammali, A. Mahsas, P. Briole, F. Benhamouda, and K. Yelles (2004), Slip distribution of the 2003 Boumerdes-Zemmouri earthquake, Algeria, from teleseismic, GPS, and coastal uplift data, *Geophys. Res. Lett.*, *31*, L18607, doi:10.1029/2004GL020687.

Deng, J., and L. R. Sykes (1997), Evolution of the stress field in Southern California and triggering of moderate-size earthquakes: A 200 year perspective, *J. Geophys. Res.*, *102*, 9859–9886, doi:10.1029/96JB03897.

Déverchère, J., et al. (2005), Active thrust faulting offshore Boumerdes, Algeria, and its relations to the 2003 M_w 6.9 earthquake, *Geophys. Res. Lett.*, *32*, L04311, doi:10.1029/2004GL021646.

Dickinson, W. R. (2002), Reappraisal of hypothetical Franciscan thrust wedging at Coalinga: Implications for tectonic relations along the Great Valley flank of the California Coast Ranges, *Tectonics*, *21*(5), 1039, doi:10.1029/2001TC001315.

Dmowska, R., J. R. Rice, L. C. Lovison, and D. Josell (1988), Stress transfer and seismic phenomena in coupled subduction zones during the earthquake cycle, *J. Geophys. Res.*, *93*, 7869–7884, doi:10.1029/JB093iB07p07869.

Freed, A. M. (2005), Earthquake triggering by static, dynamic, and postseismic stress transfer, *Annu. Rev. Earth Planet. Sci.*, *33*, 335–367, doi:10.1146/annurev.earth.33.092203.122505.

Ge, S., and S. C. Stover (2000), Hydrodynamic response to strike- and dip-slip faulting in a half-space, *J. Geophys. Res.*, *105*, 25,513–25,524, doi:10.1029/2000JB900233.

Guidoboni, E., A. Comastri, and G. Traina (1994), *Catalogue of the Ancient Earthquakes in the Mediterranean Area up to the 10th Century*, 504 pp., Inst. Naz. di Geofis., Rome.

Hardebeck, J. L., J. J. Nazareth, and E. Hauksson (1998), The static stress change triggering model: Constraints from two southern California aftershock sequences, *J. Geophys. Res.*, *103*, 24,427–24,437, doi:10.1029/98JB00573.

Harris, R. A. (1998), Introduction to special section: Stress triggers, stress shadows, and implications for seismic hazard, *J. Geophys. Res.*, *103*, 24,347–24,358, doi:10.1029/98JB01576.

Harris, R. A., R. W. Simpson, and P. A. Reasenberg (1995), Influence of static stress changes on earthquake locations in southern California, *Nature*, *375*, 221–224, doi:10.1038/375221a0.

Hearn, E. H., R. Bürgmann, and R. E. Reilinger (2002), Dynamics of Izmit earthquake postseismic deformation and loading of the Düzce earthquake hypocenter, *Bull. Seismol. Soc. Am.*, *92*, 172–193, doi:10.1785/0120000832.

King, G. C. P., R. S. Stein, and J. Lin (1994), Static stress changes and the triggering of earthquakes, *Bull. Seismol. Soc. Am.*, *84*, 935–953.

Lin, J., and R. S. Stein (2004), Stress triggering in thrust and subduction earthquakes, and stress interaction between the southern San Andreas and nearby thrust and strike-slip faults, *J. Geophys. Res.*, *109*, B02303, doi:10.1029/2003JB002607.

Ma, K.-F., C.-H. Chan, and R. S. Stein (2005), Response of seismicity to Coulomb stress triggers and shadows of the 1999 M_w = 7.6 Chi-Chi, Taiwan, earthquake, *J. Geophys. Res.*, *110*, B05S19, doi:10.1029/2004JB003389.

Magistrale, H., and S. Day (1999), 3D simulations of multisegment thrust fault rupture, *Geophys. Res. Lett.*, *26*, 2093–2096, doi:10.1029/1999GL900401.

Mahsas, A., K. Yelles, K. Lammali, E. Calais, A. M. Freed, and P. Briole (2008), Shallow afterslip following the 2003 May 21, M_w = 6.9 Boumerdes earthquake, Algeria, *Geophys. J. Int.*, *172*, 155–166, doi:10.1111/j.1365-246X.2007.03594.x.

McCloskey, J., S. S. Nalbant, and S. Steacy (2005), Indonesian earthquake: Earthquake risk from co-seismic stress, *Nature*, *434*, 291, doi:10.1038/434291a.

Meghraoui, M. (1988), Géologie des zones sismiques du nord de l'Algérie: Paléosismologie, tectonique active et synthèse sismotectonique; Ph.D. thesis, 356 pp., Paris XI Univ. Orsay, Paris.

Meghraoui, M., and F. Doumaz (1996), Earthquake-induced flooding and paleoseismicity of the El Asnam, Algeria, fault-related fold, *J. Geophys. Res.*, *101*, 17,617–17,644, doi:10.1029/96JB00650.

Meghraoui, M., S. Maouche, B. Chemaa, Z. Cakir, A. Aoudia, A. Harbi, P.-J. Alasset, A. Ayadi, Y. Bouhadad, and F. Benhamouda (2004), Coastal uplift and thrust faulting associated with the M_w = 6.8 Zemmouri (Algeria) earthquake of 21 May 2003, *Geophys. Res. Lett.*, *31*, L19605, doi:10.1029/2004GL020466.

Morel, J.-L., and M. Meghraoui (1996), Gorringe–Alboran–Tell tectonic zone: A transpression system along the Africa–Eurasia plate boundary, *Geology*, *24*, 755–758, doi:10.1130/0091-7613(1996)024<0755:GATTZA>2.3.CO;2.

Nalbant, S. S., S. Steacy, K. Sieh, D. Natawidjaja, and J. McCloskey (2005), Earthquake risk on the Sunda trench, *Nature*, *435*, 756–757, doi:10.1038/nature435756a.

Namson, J. S., and T. L. Davis (1988), Seismically active fold and thrust belt in the San Joaquin Valley, central California, *Geol. Soc. Am. Bull.*, *100*, 257–273, doi:10.1130/0016-7606(1988)100<0257:SAFATB>2.3.CO;2.

Nocquet, J. M., and E. Calais (2004), Geodetic measurements of crustal deformation in the western Mediterranean and Europe, *Pure Appl. Geophys.*, *161*, 661–681, doi:10.1007/s00024-003-2468-z.

Okada, Y. (1992), Internal deformation due to shear and tensile faults in a half-space, *Bull. Seismol. Soc. Am.*, *82*, 1018–1040.

Parsons, T. (2002), Global Omori law decay of triggered earthquakes: Large aftershocks outside the classical aftershock zone, *J. Geophys. Res.*, *107*(B9), 2199, doi:10.1029/2001JB000646.

Pollitz, F. P., P. Banerjee, R. Bürgmann, M. Hashimoto, and N. Choosakul (2006), Stress changes along the Sunda trench following the 26 December 2004 Sumatra-Andaman and 28 March 2005 Nias earthquakes, *Geophys. Res. Lett.*, *33*, L06309, doi:10.1029/2005GL024558.

Reilinger, R. E., et al. (2000), Coseismic and postseismic fault slip for the 17 August 1999, M = 7.5, Izmit, Turkey earthquake, *Science*, *289*, 1519–1524, doi:10.1126/science.289.5484.1519.

Rothé, J. P. (1950), Les séismes de Kherrata et la séismicité de l'Algérie, *Bull. Serv. Cart. Geol. Algerie, Ser. 4, Geophys.*, *3*.

Roussel, J. (1973), Les zones actives et la fréquence des séismes en Algérie 1716–1970, *Bull. Soc. Hist. Nat. Afr. Nord.*, *64*(3/2), 11–227.

Seeber, L., and J. G. Armbruster (2000), Earthquakes as beacons of stress change, *Nature*, *407*, 69–72, doi:10.1038/35024055.

Semmane, F., M. Camilo, and F. Cotton (2005), Fault location and source process of the Boumerdes, Algeria, earthquake inferred from geodetic and strong motion data, *Geophys. Res. Lett.*, *32*, L01305, doi:10.1029/2004GL021268.

Steacy, S., J. Gomberg, and M. Cocco (2005), Introduction to special section: Stress transfer, earthquake triggering, and time-dependent seismic hazard, *J. Geophys. Res.*, *110*, B05S01, doi:10.1029/2005JB003692.

Subarya, C., M. Chlieh, L. Prawirodirdjo, J.-P. Avouac, Y. Bock, K. Sieh, A. J. Meltzner, D. H. Natawidjaja, and R. McCaffrey (2006), Plate-

boundary deformation associated with the great Sumatra-Andaman earthquake, *Nature*, *440*, 46–51, doi:10.1038/nature04522.

Taylor, M. A. J., R. Dmowska, and J. R. Rice (1998), Upper plate stressing and seismicity in the subduction earthquake cycle, *J. Geophys. Res.*, *103*, 24,523–24,542, doi:10.1029/98JB00755.

Wang, J. C., C. F. Shieh, and T. M. Chang (2003), Static stress changes as a triggering mechanism of a shallow earthquake: Case study of the 1999 Chi-Chi (Taiwan) earthquake, *Phys. Earth Planet. Inter.*, *135*, 17–25, doi:10.1016/S0031-9201(02)00175-9.

Wang, W. H., and C. H. Chen (2001), Static stress transferred by the 1999 Chi-Chi, Taiwan, earthquake: Effects on the stability of the surrounding fault systems and aftershock triggering with a 3D fault-slip model, *Bull. Seismol. Soc. Am.*, *91*, 1041–1052, doi:10.1785/0120000727.

Wessel, P., and W. H. F. Smith (1998), New, improved version of generic mapping tools released, *Eos Trans. AGU*, *79*(47), 579.

Yelles, K., K. Lammali, A. Mahsas, E. Calais, and P. Briole (2004), Coseismic deformation of the May 21st, 2003 earthquake, Algeria, from GPS measurements, *Geophys. Res. Lett.*, *31*, L13610, doi:10.1029/2004GL019884.

A. Ayadi, Centre de Recherche en Astronomie Astrophysique et Geophysique, Route de l'Observatoire, Bouzareah, Algiers 16340, Algeria.

S. Belabbes, SERTIT, Boulevard Sébastien Brant, BP 10413, F-67412 Illkirch, France.

C. Dorbath and M. Meghraoui, Institut de Physique du Globe de Strasbourg, EOST, 5, rue Rene Descartes, F-67084 Strasbourg, France.

J. Lin, Department of Geology and Geophysics, Woods Hole Oceanographic Institution, 255 Woods Hole Rd., Woods Hole, MA 02543, USA. (jlin@whoi.edu)

R. S. Stein, U.S. Geological Survey, 345 Middlefield Rd., MS 977, Menlo Park, CA 94025, USA.

S. Toda, Disaster Prevention Research Institute, Kyoto University, Gokasyo, Uji, Kyoto 611-0011, Japan.